

Hysteretic damping in a small-strain stiffness model

R.B.J. Brinkgreve

Delft University of Technology & Plaxis bv, Delft, The Netherlands

M.H. Kappert

Twente University of Technology, Enschede, The Netherlands

P.G. Bonnier

Plaxis bv, Delft, The Netherlands

ABSTRACT: This paper shows the results of a study in which the new Plaxis Hardening Soil model with small-strain stiffness (HSsmall) was analyzed with respect to its hysteretic damping characteristics for dynamic applications. An analytical expression was derived to formulate the local damping ratio as a function of the local shear strain. Results are shown for common ranges of parameters. Subsequently, the model with an existing parameter data set for Kaolin was used in dynamic finite element calculations and subjected to cyclic loading at different strain levels as well as free vibration. The results were compared with the analytical expression. A comparison was made with experimental data on damping, and another comparison was made with Rayleigh damping, which is commonly used in simple models. From the results it was concluded that HSsmall model has indeed some potential for dynamic applications. However, it does not yet capture material damping at small strain levels (for which Rayleigh damping or viscous damping may be added), and it does not include the accumulation of strain (or pore pressure) with multiple load cycles.

1 INTRODUCTION

In a former research project (Benz, 2006; Benz et al. 2006) an extension was made to the Plaxis Hardening Soil (HS) model (Schanz, 1998) in order to cope with the high-stiffness behaviour that geo-materials show when subjected to very small strains. The resulting model (HSsmall, as it is called) has been tested extensively in various static applications to demonstrate its usefulness for the geotechnical engineering applications (e.g. Brinkgreve et al. 2006). Although the model has not been designed specifically for dynamic applications, it does have capabilities to describe dynamic soil behaviour to some extent. The small-strain stiffness formulation involves the degradation of the shear stiffness with the shear strain, and it takes into account that the high small-strain stiffness is regained upon load reversal. When subjected to cyclic shear loading the model shows hysteresis. This feature provides damping in dynamic applications.

This paper shows the results of a recent study in which the HSsmall model has been further analyzed and tested in order to evaluate its damping characteristics in dynamic applications. Chapter 2 gives a brief description of the model. In Chapter 3 the hysteretic

damping characteristics of the model are analytically derived based on the small-strain stiffness formulation. Chapter 4 demonstrates the results of the derived expression for a common range of parameter values. Chapter 5 shows a numerical verification example based on an existing HSsmall data set for Kaolin clay. For load cycles at different strain levels as well as for free vibration the damping observed from the numerical results is compared with the analytical expression as derived in Chapter 3. In Chapter 6 the behaviour of the data set is compared with empirical observations. Chapter 7 shows a comparison with Rayleigh damping, which is generally used in models that do not include damping in the constitutive relation. The final Chapter 8 gives the conclusions of this study.

2 SMALL-STRAIN STIFFNESS MODEL

The HSsmall model is based on the Plaxis Hardening Soil model, extended with an elastic overlay model to take into account the high stiffness at small strain levels. The model has been implemented in the finite element program Plaxis (version 8.4). The extra information that is needed for the small-strain stiffness

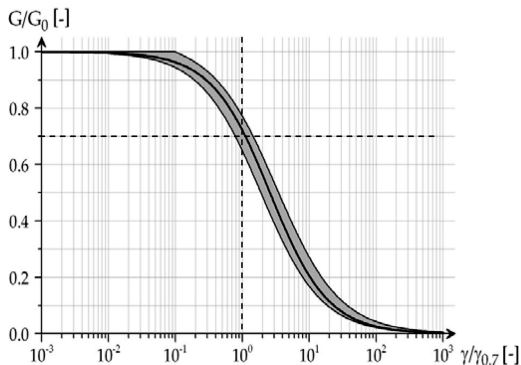


Figure 1. Reduction of secant shear modulus with shear strain.

formulation comes from modulus reduction curves where the shear modulus, G , is plotted as a logarithmic function of the shear strain, γ , ranging from very small strain levels (vibrations) up to large strain levels. In the HSsmall model the reduction curve is characterized by the small-strain shear modulus, G_0 , and the shear strain at which the secant shear modulus has reduced to 0.7 times G_0 ($\gamma_{0.7}$); Fig. 1. The two parameters G_0 and $\gamma_{0.7}$ are the only extra parameters compared to the original HS model. In fact, it has been demonstrated by comparing curves of several different types of soil that the particular shape of the curve does not change much and that $\gamma_{0.7}$ is generally between 1 and 2 times 10^{-4} . G_0 generally ranges from around 10 times G_{ur} for soft soils, down to 2.5 times G_{ur} for harder types of soil, where $G_{ur} = E_{ur}/(2(1 + \nu_{ur}))$.

The decay of the secant shear modulus depends on the amount of shear strain as depicted in Fig. 1. A good approximation is given by Eq. 1.

$$G_s = \frac{G_0}{1 + a\gamma/\gamma_{0.7}} \quad (1)$$

The constant a is set to 0.385 to arrive at the best fit (central line Fig. 1). It should be noted that the curve shows the secant shear modulus, not the tangent shear modulus. From the secant shear modulus the stress-strain relationship can simply be formulated as:

$$\tau = G_s \gamma = \frac{G_0 \gamma}{1 + a\gamma/\gamma_{0.7}} \quad (2)$$

Taking the derivative with respect to the shear strain gives the tangent shear modulus:

$$G_t = \frac{G_0}{(1 + a\gamma/\gamma_{0.7})^2} \geq G_{ur} \quad (3)$$

The curve in Fig. 1 reaches far into the plastic domain. As the HSsmall model is an overlay model, the tangent shear modulus is bounded by a lower limit, G_{ur} , of the original HS model. When combined with the HS model, the apparent shear modulus will reduce further due to plasticity. As for the original HS model, plasticity occurs due to an isotropic shear hardening surface and an isotropic cap hardening surface.

The model is primarily meant for shear stiffness reduction. The bulk modulus is calculated from the shear modulus using a fixed elastic Poisson's ratio.

$$K_t = \frac{2(1 + \nu)}{3(1 - 2\nu)} G_t \quad (4)$$

So far, only continuous loading was considered but in practice the stiffness increases when the loading direction changes. For a full '180 degrees' load reversal, the stiffness is supposed to restart at its maximum. For a new strain path that is in between a continuation in the same direction and a full load reversal, an intermediate (interpolated) stiffness is assumed. Therefore, the small-strain stiffness model memorizes the 'deviatoric' strain history and uses a generalized shear strain parameter to evaluate to what extend the loading direction deviates from the strain history. On the basis of this information it is determined which stiffness should be used. More details about the precise formulation of this generalized small-strain stiffness concept can be found in Benz, 2006.

3 HYSTERETIC DAMPING

When subjected to cyclic shear loading, the HSsmall model will show typical hysteretic behaviour as visualized in Fig. 2. Starting from the small-strain shear stiffness, G_0 , the actual stiffness will decrease with increasing shear strain according to Fig. 1. Upon load reversal the stiffness will restart from G_0 and will decrease again until the next load reversal.

Underneath we will consider cyclic shear loading until a particular magnitude of cyclic shear strain γ_c . From the above expressions (1-3), after some elaboration, the dissipated energy in a load cycle from $\gamma = -\gamma_c$ to $+\gamma_c$ and back to $-\gamma_c$, equivalent with the area of the closed loop in Fig. 2, can be formulated as:

$$E_D = \frac{4G_0\gamma_{0.7}}{a} \left(2\gamma_c - \frac{\gamma_c}{1 + \gamma_{0.7}/a\gamma_c} - \frac{2\gamma_{0.7}}{a} \ln \left(1 + \frac{a\gamma_c}{\gamma_{0.7}} \right) \right) \quad (5)$$

Now, the local hysteretic damping ratio, ξ , can be defined as:

$$\xi = \frac{E_D}{4\pi E_s} \quad (6)$$

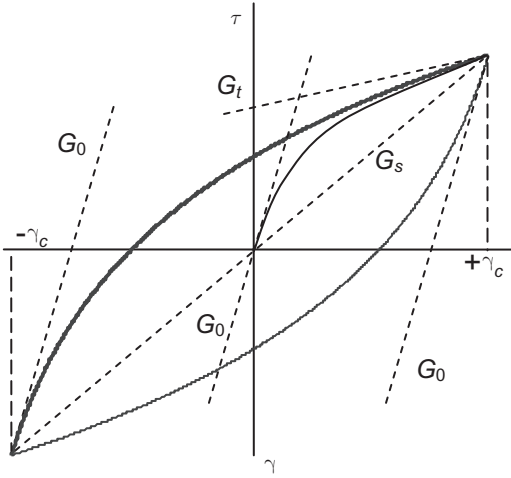


Figure 2. Hysteretic behaviour in the HSsmall model.

where E_s is the energy stored at maximum strain γ_c :

$$E_s = \frac{1}{2} G_s \gamma_c^2 = \frac{G_0 \gamma_c^2}{2 + 2a \gamma_c / \gamma_{0.7}} \quad (7)$$

This holds as long as G_{ur} has not been reached, i.e.:

$$\gamma_c \leq \frac{\gamma_{0.7}}{a} \left(\sqrt{G_0 / G_{ur}} - 1 \right) \quad (8)$$

The above damping ratio in the HS small model only applies as long as the material behaviour remains elastic and the shear modulus decreases according to the small-strain formulation. As soon as G_{ur} is reached the damping does not further increase. On the other hand, as soon as (hardening) plasticity occurs, the observed damping will further increase. In both cases the above equations do not apply anymore.

It should also be noted that the above damping ratio is independent from the loading frequency, since the derivation in this paragraph is purely based on the stress-strain relationship, which is time-independent.

4 PARAMETER VARIATIONS

On the basis of the above equations a simple parametric study was performed to evaluate the range of damping ratios that can be expected from realistic combinations of small-strain parameters. Fig. 3 shows the damping ratio as a function of the cyclic shear strain γ_c for different values of $\gamma_{0.7}$ [$1 \cdot 10^{-4} - 3 \cdot 10^{-4}$] and different G_0/G_{ur} ratios [2.5–10].

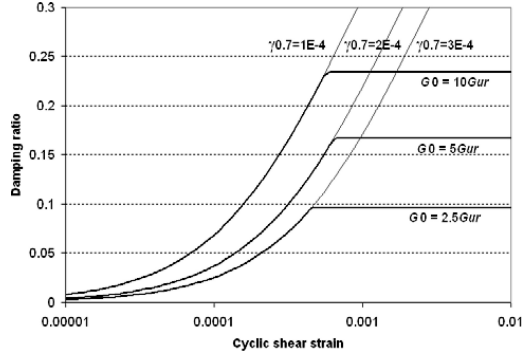


Figure 3. Damping ratio ξ as a function of cyclic shear strain γ_c .

Table 1. HS small material data set for Kaolin (after Benz).

Parameter	Symbol	Value	Unit
Unsaturated unit weight	γ_{unsat}	11.3	kN/m ³
Saturated unit weight	γ_{sat}	17.0	kN/m ³
Small strain stiffness	G_0^{ref}	33300	kN/m ²
Shear strain at 0.7 G_0	$\gamma_{0.7}$	$2 \cdot 10^{-4}$	–
Poisson's ratio	ν_{ur}	0.2	–
Triaxial compression stiffness	E_{50}^{ref}	1500	kN/m ²
Primary oedometer stiffness	E_{oed}^{ref}	750	kN/m ²
Unloading/reloading stiffness	E_{ur}^{ref}	8000	kN/m ²
Reference pressure	p^{ref}	100	kN/m ²
Rate of stress-dependency	m	1.0	–
Cohesion	c	0.0	kN/m ²
Friction angle	φ	21.0	°
Dilatancy angle	ψ	0.0	°
Failure ratio	R_f	0.9	–
Stress ratio in primary compr.	K_0^{nc}	0.64	–

Regarding the variation of $\gamma_{0.7}$ it can be seen that a lower $\gamma_{0.7}$ gives more damping, or damping occurs at smaller shear strain. On the other hand, a variation of G_0/G_{ur} only leads to a different maximum damping ratio, regardless the selected value of $\gamma_{0.7}$. When the difference between G_0 and G_{ur} (i.e. the difference between the upper bound and lower bound G -value) is larger, the maximum damping is also larger. The maximum damping for a particular combination of parameters can be obtained from Eq. 6 by substituting the maximum shear strain according to Eq. 8.

5 EXAMPLE

In this paragraph a numerical example will be considered. The example is performed with an existing HS small material data set representing soft Kaolin clay with a plasticity index of 30%, as reported by Benz (2006). The full material data set is listed in Table 1.

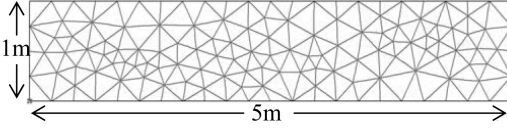


Figure 4. Finite element mesh composed of 15-node elements.

From the above data, the following auxiliary parameters for dynamic application can be determined:

$$G_{ur}^{ref} = E_{ur}^{ref} / (2(1+\nu_{ur})) = 3330 \text{ kN/m}^2$$

$$G_0/G_{ur} = 10$$

Shear wave velocity at p^{ref} :

$$c_s = \sqrt{(G_0^{ref} / \rho)} = 170.0 \text{ m/s}$$

Compression wave velocity at p^{ref} :

$$c_p = \sqrt{(E_{oed0}^{ref} / \rho)} = 277.6 \text{ m/s}$$

where E_{oed0}^{ref} is the oedometer stiffness at small strains and ρ is the density ($\gamma_{unsat}/9.81$).

$$E_{oed0}^{ref} = 2G_0^{ref} (1-\nu_{ur}) / (1-2\nu_{ur}) = 88800 \text{ kN/m}^2$$

The example being considered is a 1 m thick clay layer subjected to shearing. Soil self weight is not considered, but an effective confining pressure of 100 kN/m² is applied around the layer. To ensure that the behaviour is purely elastic, a preloading (compression as well as deviatoric loading) is applied and removed before the intended shear loading.

Fig. 4 shows the 5 × 1 m² finite element mesh composed of 15-node (cubic strain) triangular elements that has been used for the analysis.

To verify the hysteretic behaviour in the numerical model, cyclic shearing has been simulated in a dynamic finite element analysis by imposing a prescribed displacement at the bottom boundary while leaving the other boundaries free (with confining pressure). In this way a number of load cycles were applied at different shear strain levels. To avoid dynamic amplification a loading frequency of 10 Hz has been selected, which is well below the model's natural frequency (≈ 35 Hz). The damping (dissipated energy in the hysteresis loop) obtained from the numerical model compares well with the analytical results (see Fig. 5). In addition, an initial shear loading has been applied at the top of the model and then released in a dynamic calculation. The resulting natural cyclic movement (free vibration) at the upper side is visualized in Fig. 6.

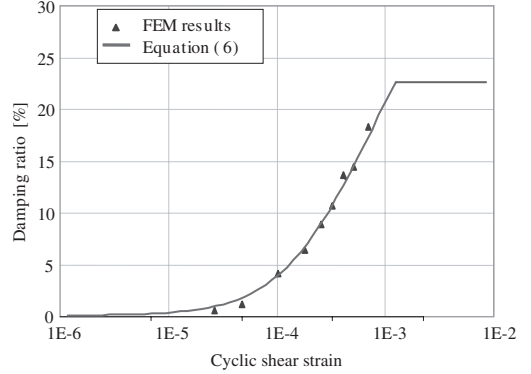


Figure 5. Verification of damping for different strain levels.

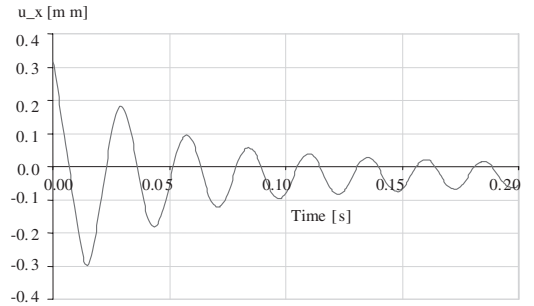


Figure 6. Natural cyclic movement after release of shear load.

The reduction of the displacement amplitude in two successive cycles relates to the damping ratio in the following way:

$$\xi = \frac{\omega_D}{2\pi\omega_0} \ln\left(\frac{u_k}{u_{k+1}}\right) = \frac{\ln(u_k/u_{k+1})}{\sqrt{(2\pi)^2 + \ln(u_k/u_{k+1})^2}} \quad (9)$$

where ω_0 is the eigen-frequency, ω_D is the damped frequency and u_k is the horizontal displacement amplitude in cycle k . From this expression and the results in Fig. 6 the damping ratio can be back-analyzed for different levels of cyclic shear strain. Fig. 7 shows a comparison with the damping ratio according to Eq. 6. At low strain levels the observed damping is less than the theoretical value, whereas at higher strain levels the results match reasonably well. After a few cycles the strain level becomes so small that there is hardly any further damping, so that the free vibration continues more than observed in reality.

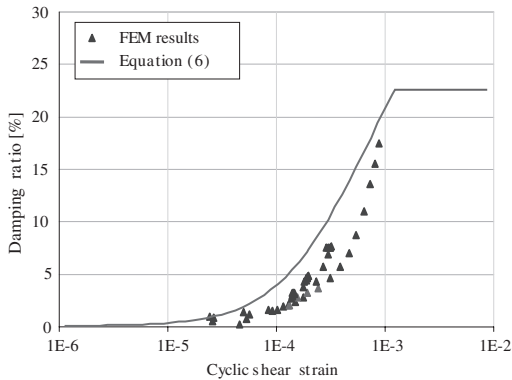


Figure 7. Verification of damping from free vibration.

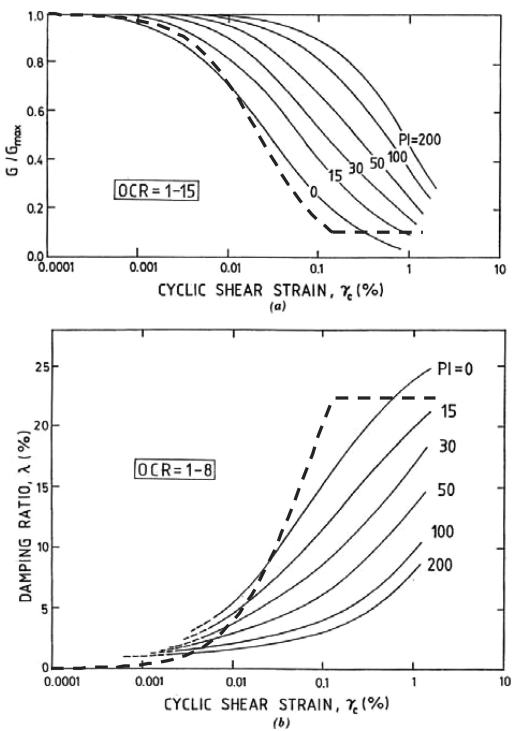


Figure 8. Small-strain stiffness and damping ratio for clays with different plasticity index (after Vucevic et al. 1991). The dashed line corresponds to the Kaolin data set in Table 1.

6 COMPARISON WITH EMPIRICAL DATA

Vucevic & Dobry (1991) have compiled empirical data on small-strain stiffness and material damping for different types of clay, using the plasticity index as a reference parameter. Fig. 8 shows this data, with the results for the Kaolin data set superimposed on it as a

dashed line. The upper graph indicates that for Kaolin with a plasticity index of 30% the stiffness reduction should occur later than modelled by the data set in Table 1. This would suggest the use of a higher value of $\gamma_{0.7}$. On the other hand, the lower graph indicates that at lower strain levels there is more damping in reality than modelled by the data set. The latter cannot be solved by a different value of $\gamma_{0.7}$, but requires additional damping independent from the strain level (viscous or Rayleigh damping).

7 COMPARISON WITH RAYLEIGH DAMPING

Apart from hysteretic material damping, damping can be modelled in general by means of Rayleigh damping. Rayleigh damping can be regarded as a ‘trick’ to add viscous damping, since it contributes to the velocity term in the dynamic equation by taking a portion of mass ($\alpha \underline{M}$) and a portion of stiffness ($\beta \underline{K}$), where \underline{M} is the mass matrix, \underline{K} is the stiffness matrix and α and β are the Rayleigh coefficients.

In contrast to hysteretic damping, Rayleigh damping is frequency-dependent. Hence, before selecting the Rayleigh coefficients to arrive at a particular damping ratio, a range of target frequencies must be selected in accordance with the natural frequency of the system and the dominant load frequency.

For the example as considered in Section 5 (free vibration after release of an initial shear load) an alternative calculation has been performed using the standard Hardening Soil model without small-strain stiffness, and thus without hysteretic damping, but using Rayleigh damping instead. Again, hardening during the dynamic application was excluded by preloading and unloading the sample in compression and shear before applying the free vibration.

The Rayleigh coefficients were based on a damping ratio of 11.2% (average in the previous example) and a target frequency between 10 Hz and 35 Hz, giving $\alpha = 10.946$ and $\beta = 7.928 \cdot 10^{-4}$. The resulting natural cyclic movement at the upper side of the model with Rayleigh damping is visualized in Fig. 9. Again, the damping ratio can be back-analyzed using Eq. 9, which indeed gives damping ratios around 11.2% (except for the first cycle).

In contrast with the previous example with hysteretic damping where the damping ratio was found to be dependent on the strain level, the current example shows a more or less constant damping ratio which is typical for viscous damping. Moreover, the natural vibration seems, to some extent, to be influenced by the damping. As a result, the total picture is significantly different, although it was intended that the results from both cases would match. In conclusion, Rayleigh damping cannot be used as an alternative for hysteretic material damping. However, it can be

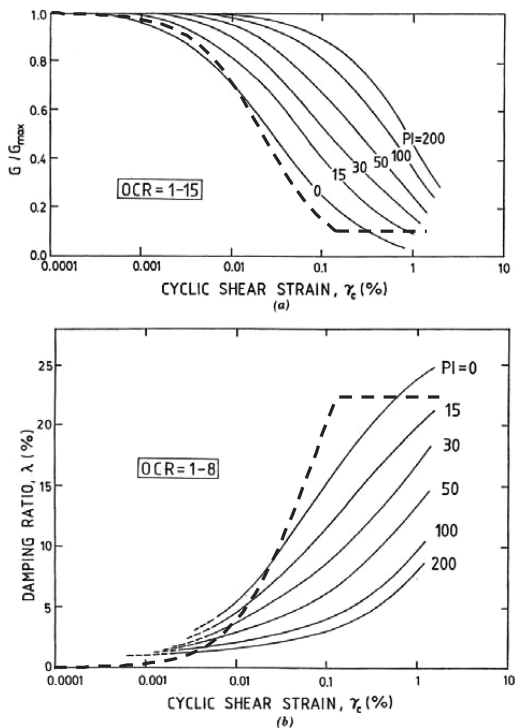


Figure 9. Natural cyclic movement with Rayleigh damping.

added to hysteretic damping to provide at least a small amount of damping at small strain levels.

8 CONCLUSIONS

This paper demonstrates that the Plaxis Hardening Soil model with small-strain stiffness (HSsmall) has capabilities to model hysteretic damping in dynamic applications. An analytical expression has been derived for the damping ratio based on the stiffness reduction curve. Results were shown for different combinations of realistic model parameters. The analytical results

were also used to verify the numerical implementation of the model on the basis of an existing data set for Kaolin. The numerical results for constant load cycles were found to match the analytical expression nicely, whereas the numerical results based on free vibration show a deviation at the high strain levels in the first cycles. Moreover, a comparison has been made with empirical data from Vucevic et al. From this comparison it can be concluded that, in order to model damping even more realistically, a higher value of $\gamma_{0.7}$ should be used and viscous damping should be added. Finally, a comparison has been made between hysteretic damping and Rayleigh damping. From this analysis it was concluded that Rayleigh damping can not be used as an alternative for hysteretic damping, but that it can be added to hysteretic damping to provide at least a small amount of damping at small strain levels. Finally, it should be mentioned that the current HSsmall model does not allow for accumulation of strain or pore pressure with cyclic loading. The latter will be considered in the near future.

REFERENCES

- Benz, T. 2006. *Small-strain stiffness of soils and its numerical consequences*. Ph.D. Thesis. Institut für Geotechnik, Universität Stuttgart.
- Benz, T., Schwab, R. and Vermeer, P.A. 2006. *A small strain overlay model I: model formulation*. Int. J. Numer. Anal. Meth. Geomech., in progress.
- Brinkgreve, R.B.J., Bakker, K.J. and Bonnier, P.G. 2006. *The relevance of small-strain stiffness in excavation and tunnelling projects*. In: H.F. Schweiger (ed.) Numerical Methods in Geotechnical Engineering. Taylor & Francis. 133–139.
- Kappert, M.H. 2006. *Hysteretic damping in the hardening Soil small strain model*. Graduation thesis. Twente University of Technology.
- Schanz, T. 1998. *Zur Modellierung des Mechanischen Verhaltens von Reibungsmaterialien*. Habilitation. Stuttgart University.
- Vucevic, M. and Dobry R. 1991. *Effect of soil plasticity on cyclic response*. Journal of Geotechnical Engineering, ASCE, 117(1): 89–107.